Future Generation Computer Systems 95 (2019) 713–726

Contents lists available at ScienceDirect

Future Generation Computer Systems

journal homepage: www.elsevier.com/locate/fgcs

A multi-hop routing protocol for video transmission in IoVs based on cellular attractor selection

Daxin Tian [a,b], Chuang Zhang [a], Xuting Duan [a,b,*], Yunpeng Wang [a,b], Jianshan Zhou [a], Zhengguo Sheng [c]

[a] Beijing Advanced Innovation Center for Big Data and Brain Computing, Beijing Key Laboratory for Cooperative Vehicle Infrastructure Systems and Safety Control, School of Transportation Science and Engineering, Beihang University, Beijing 100191, China
[b] Jiangsu Province Collaborative Innovation Center of Modern Urban Traffic Technologies, SiPaiLou # 2, Nanjing, 210096, China
[c] Department of Engineering and Design, the University of Sussex, Richmond 3A09, UK

HIGHLIGHTS

- We propose a multi-hop routing protocol for video transmission in IoVs based on cellular attractor selection (MRVT-CAS)
- We design a packet generation method for MRVT-CAS and use Technique for Order Preference by Similarity to an Ideal Solution (TOPSIS) to construct the candidate set of next-hop selection.
- We map the expression of different genes in cell to selection of different next-hop nodes, and employ the mechanics of cellular attractor selection to select next-hop node.
- We present a real-time feedback process to improve self-adaptability and robustness of routing protocol.
- The simulation results demonstrate the performance improvement over traditional methods, in terms of reachability, delay, stability and frame loss rate.

ARTICLE INFO

Article history:
Received 29 July 2018
Received in revised form 19 September 2018
Accepted 29 September 2018
Available online 30 January 2019

Keywords:
Internet of vehicles
Vehicle Ad Hoc Networks
Video transmission
Cellular attractor selection
Real-time feedback

ABSTRACT

Video transmission in Internet of Vehicles (IoVs) is an emerging technology which utilizes the multimedia inside and outside vehicles itself through Vehicle Ad Hoc Networks (VANETs). In IoVs, traditional multi-hop routing protocols are not adaptive to mobile environment, especially the high-mobility driving environment in which vehicles need to accomplish video transmission under high quality of service (QoS). In this paper, we propose a multi-hop routing protocol for video transmission in IoVs based on cellular attractor selection (MRVT-CAS). We design a packet generation method for MRVT-CAS and use Technique for Order Preference by Similarity to an Ideal Solution (TOPSIS) to construct the candidate set of next-hop selection. Then we map the expression of different genes in cell to selection of different next-hop nodes, and employ the mechanics of cellular attractor selection to select next-hop node. Moreover, we present a real-time feedback process to improve self-adaptability and robustness of routing protocol. Our simulation study compares MRVT-CAS with other routing protocols to evaluate performance of video transmission. The simulation results demonstrate the performance improvement over traditional methods, in terms of reachability, delay, stability and frame loss rate.

1. Introduction

With the development of communication and computer technologies, IoVs (Internet of Vehicles) has been developed rapidly in recent years [1]. As a vital important part of IoVs, the Vehicle Ad Hoc Networks (VANETs) have become one of research hotspots in the field of communication and transportation [2,3]. The transmission of message in VANETs has enabled many applications, such as cooperative collision avoidance, lane change assistance, traffic accident information broadcasting [4,5]. But now more and more drivers dissatisfy these applications only based on message, and they have demand for more realistic applications based on video, such as obtaining real-time traffic waring video, accessing road video remotely and video sharing between vehicles [6,7]. Therefore, many studies and projects have been launched for developing video transmission in IoVs [8–10].

In IoVs, a source node is often far away from a destination node, and there are many intermediate nodes in the process of data

* Corresponding author at: Beijing Advanced Innovation Center for Big Data and Brain Computing, Beijing Key Laboratory for Cooperative Vehicle Infrastructure Systems and Safety Control, School of Transportation Science and Engineering, Beihang University, Beijing 100191, China.
E-mail address: duanxuting@buaa.edu.cn (X. Duan).

https://doi.org/10.1016/j.future.2018.09.070
0167-739X/

transmission. Therefore, the performance of multi-hop routing protocols directly affects the efficiency and quality of data transmission. As a special type of mobile ad hoc networks (MANETs), VANETs have a more highly dynamic nature because of the fast moving of vehicles [11]. In addition, VANETs may not have full connection at all times when the traffic density is low. On account of the highly dynamic topology, frequent disconnection, changing traffic density and massive packets, some MANETs routing protocols depending on the maintenance of an end-to-end transmission path cannot work well in VANETs [12,13]. Moreover, there are a large number of continuous packets transmitted simultaneously for video transmission in IoVs. Besides, the condition of each vehicle in the IoVs is different, in terms of location, speed and number of packets carried, which have influence on transmission performance. Therefore, some routing protocols in VANETs that select next-hop only relying on position information of vehicles will fail to work well for video transmission in IoVs, which may cause the serious congestion of some nodes in short time [14].

In general, the data packets transmission in IoVs is similar with behavior of E. coli cells' gene network in a varying environment, which is discovered by Kashiwagi [15]. For instance, both the VANETs and living environment of cells are complex and highly dynamic. Then VANETs and cells all need adjust themselves to adapt to the changes in the environment. For cells, they can adjust themselves by controlling the expression of different genes. And VANETs can adjust themselves based on dominating the selection of different next-hop node in multi-hop routing path. Under this background, we have already done some works in combining E. coli cells and VANETs [16–19], and we also proposed some routing protocols for VANETs. However, these routing protocols are not suitable for video transmission in IoVs because of inappropriate feedback process and lower ability to deal with massive packets.

In this paper, we propose a multi-hop routing protocol for video transmission in IoVs based on some adaptive forwarding mechanisms and biologically inspired models, whose goal is improving efficiency and quality of video transmission in IoVs. With the goal, we focus on such a general application scenario that some specific vehicles intend to send their video captured by vehicular camera to other certain vehicles. First, a method of video data packets generation based on H264 [20] and Real-time Transport Protocol (RTP) [21] is designed to improve their applicability for video transmission in IoVs. Then we combine TOPSIS with entropy weight method to construct the candidate set of next-hop node selection. Third, we map the expression of different genes in cell to selection of different next-hop vehicle nodes, and use extended cellular attractor selection method to select next-hop node in candidate set. Last, a real-time feedback method based on performance of next-hop selection process is developed to enhance MAVT-CAS's self-adaptability and robustness for video transmission in IoVs.

The rest of this paper is organized as follows: Section 2 gives an overview of some related work. Section 3 describes the proposed method MRVT-CAS in detail. Section 4 discusses performance comparison of MRVT-CAS and other routing protocols. Finally, Section 5 concludes this paper.

2. Related work

The multi-hop routing protocol for video transmission in IoVs is a challenging issue and has attracted considerable attention from researchers. They have proposed and applied various routing methods, such as Dynamic Source Routing (DSR) [22,23] and Ad hoc On-Demand Distance Vector routing (AODV) [24,25]. These two methods are passive route protocol, they only can adapt to some specific scenarios and will cause serious end-to-end delay. From experiment results of video transmission in IoVs in [23], it can be found that DSR can work well when the order of the vehicles is constant and every two adjacent vehicles keep communication all the time. In fact, this scenario is hard to be obtained in real IoVs because of frequent overtaking and long distance between adjacent vehicles in low density traffic flows. [25] uses AODV augmented with the expected transmission count (ETX) metric to find the best quality route, and it can be found that this method needs to restart to discover new routing path if current path is broken. Therefore, the routing methods based AODV will result in serious delay when the traffic density is heavy and the vehicle motion condition is changing fast. There are also some other methods which use the local statistical information. Distribution-Adaptive Distance with Channel Quality (DADCQ) protocol is presented in [26], which is a Distance-based Statistical Routing Protocol (SRP) that is adaptive to distribution pattern and channel quality for multi-hop V2V broadcast. Dynamic Backbone Assisted (DBA) protocol is proposed in [27], which is a contention-based protocol for multimedia flooding in VANETs and uses positioning and QoS-based parameters, such as link quality, vehicles location and speed. The cross-layer QOe-driven REceiver-based (QORE) mechanism is presented in [28], which is modularly coupled to SRPs to offer QoE-aware and video-related parameters for the relay node selection and backbone maintenance. These statistical-based methods usually rely on several parameters to decide whether a vehicle node should forward or discard revived data packets. Moreover, there are many geometric-based routing methods, such as Position-Based Routing (PBR) [29], Geographic Source Routing (GSR) [30] and Greedy Predictive Stateless Routing (GPSR) [31]. These methods usually presume the accessibility of traffic parameters, such as vehicle position and speed. GPSR is utilized to transmit data packets in IoVs in [32], and the experiment results show that GPSR cannot work well even transmission rate is low. It is not suitable for video transmission in IoVs. That is because there are hundreds of data packets sent from video resource node to video demand node per second, and the GPSR always selects the node that is closest to demand node as next-hop node. It causes some nodes accumulate many data packets in a short time and cost a long time to forward these data packets, which increases the delay and decreases the delivery rate. What is more, it is worse if there are multiple pairs of resource–demand nodes transmitting video simultaneously.

As mentioned in Section 1, considering the similarities between E. coli cells and VANETs, we have already done some works by combining them together. [16] has extended the basic two-dimensional cellular attractor selection model (CASM) in [15] to the high-dimensional space, which is named as extended attractor selection model (EASM). In [19], the unicast routing protocol based the EASM (URAS) is proposed to transmit message in IoVs, which takes into consideration some parameters of vehicle motion and routing performance, such as vehicle velocity, delay and congestion. The simulation results show that URAS outperforms the GPSR in terms of delay, congestion and delivery rate. However, URAS is unsuitable for video transmission in IoVs. URAS regards all nodes in a routing path as a cell and updates the selected possibility of these nodes after this routing path finish, which will cause the problem of selected possibility updating too late in process of video transmission. This delay of information updating also causes many nodes to be in a state of massive congestion. Moreover, URAS aims only high packet delivery rates and low end-to-end delay levels, without addressing the subjective acceptability of users when watching the video stream.

Concerning the core issue mentioned above, for sake of avoiding congestion in GPSR, our proposed MRVT-CAS takes into consideration several parameters of vehicle motion and vehicle communication instead of only vehicle position. Moreover, in order to reduce the delay of information updating, MRVT-CAS regards current node and its neighbor nodes as a cell and utilizes a real-time feedback process to update the selected possibility after each selection of next-hop node.

3. Multi-Hop Routing Protocol for Video Transmission Based on Cellular Attractor Selection (MRVT-CAS)

MRVT-CAS is a multi-hop routing protocol for video transmission in IoVs based on the cellular attractor selection. The schematic diagram of MRVT-CAS is shown in Fig. 1. The left part of the figure is a complex road network. Black lines represent roads, and black dots represent intersections. There is a path of MRVT-CAS in this part, the green dot represents video resource node, the blue dot represents video demand node, and the red dots represent intermediate nodes. The middle part of the figure is three detail descriptions of MRVT-CAS. For the process of next-hop node selection, the vehicle set including current node and other nodes in communication range of current node is regarded as a cell. We map the expression of different genes in cell to selection of different next-hop nodes. The right part of figure is specific process of next-hop node selection, including constructing candidate set by TOPSIS and determining the next-hop node by cellular attractor selection.

The rest of this Section describes the data structures and algorithms in detail.

3.1. Data structures

There are three data structures in MRVT-CAS, including two types of data packet and a type of node attribute table.

(1) VDDP
VDDP is the data packet sending from video demand node to video resource node, and the structure of VDDP is shown in Table 1. There are many kinds of data packets in Internet of vehicles, including signal information packets, vehicle safety information packets and so on. So, the first part of VDDP is set as DPT (Data Packets Type), which enables vehicle take different actions for receiving different kinds of data packets. The following part is VDDP.H (VDDP Header), including VDDP ID, data packet length, demand node ID and resource node ID. The third part is RI (Routing Information), which is used to store the information about VDDP arriving time and VDDP sending out time of intermediate nodes. The last part is CC (Control Command), which enables demand node control the video stream to start, pause, and stop.

(2) VDP
VDP is the data packet sending from video resource node to video demand node, and the structure of VDP is shown in Table 2. The first, second and third parts of VDP are same as VDDP. The fourth part is RTP.H (RTP Header), including format of video stream, serial number and time stamp. The fifth part is NALU.H (NALU Header), and the last part is NALU.D (NALU Data). Because of the different encoding methods, the size of frames in the encoded video stream is different. So we use two schemes to generate VDP, and these two schemes are corresponding to different NALU header.

- Single NALU Packet
  If the size of current frame is less than 1400B, the NALU corresponding to this frame is stored in a single VDP. In this case, the NALU header includes two parts. The first one is F, which enables demand node abandon this VDP when there are mistakes in current NALU. The second part is Type, which contains the type information of current NALU.
- Fragmentation Unit NALU Packet
  If the size of current frame is not less than 1400B, the NALU corresponding to this frame is divided into several fragments. Every fragment is stored in a VDP, and these several VDPs are called Fragmentation Unit of current NALU. In this case, the NALU header includes four parts. The first part is F, and the second part is Type. The third part is S, which is used to distinguish whether the packet is the starting VDP of current NALU. The last part is E, which is used to distinguish whether the packet is the ending VDP of current NALU.

Table 1
The structure of VDDP.

DPT	VDDP.H	RI	CC

Table 2
The structure of VDP.

DPT	VDP.H	RI	RTP.H	NALU.H	NALU.D

(3) NAT
NAT(Node Attribute Table) is used to store motion parameters and cellular attractor indexes of vehicle nodes. It includes node location, node velocity, number of data packets carried by node, the cell activity of node set and the probability that each node is selected as the next-hop node. This table offers basic data for constructing candidate set and selecting next-hop node.

3.2. Construction of candidate set based on TOPSIS

In IoVs, there are many vehicles in communication range of current vehicle node i, and these vehicles make up the neighbor vehicle set V_i of i. If using the cell attractor selection model to select the next-hop node in V_i directly, it will ignore the influence of vehicle motion factors and greatly increase the randomness of the selection, which is unfavorable to the stability and efficiency of video stream transmission. So we develop a multi-attribute decision-making method based on TOPSIS. This method scores each vehicle c in V_i, and select top ten vehicles to construct next-hop candidate set VC_i of i. This method considers four attributes, including

- Number of data packets carried by c, DN_c. DN_c has a great impact on video transmission, and the larger DN_c indicates that c have a lot of packets waiting for transmission. If i selects this c as the next-hop node, it will cause the current data packet to wait for a long time to be forwarded.
- Relative velocity of c and demand node, v_{cd}. The higher v_{cd} implies that the current data packet has a good potential to be delivered to demand node with a shorter delay.
- Relative distance of c and demand node, Dis_{cd}. The smaller Dis_{cd} implies that current data packet has a high possibility to be delivered to demand node with a fewer hops.
- Number of vehicles in communication range of c, NV_c. If there are few vehicles in communication range of c, it is difficult for c to find a next-hop node with good performance.

This method of constructing candidate sets includes the following steps.

(1) Construction of initial decision matrix DM_i.
The larger DN_c and Dis_{cd} go against the performance of video transmission, while the larger v_{cd} and NV_c are significant to it. In order to unify the effect of attributes monotonicity on the transmission performance, v'_{cd} and NV'_c in Eq. (1) are used to replace v_{cd} and NV_c. Let number of vehicles in V_i is n, and each vehicle has four attributes DN_c, Dis_{cd}, v'_{cd}, NV'_c. These data form initial decision matrix DM_i, and its size is $n * 4$.

$$\begin{aligned} v'_{cd} &= \max_{c \in V_i} \{v_{cd}\} - v_{cd} \\ NV'_c &= \max_{c \in V_i} \{NV_c\} - NV_c \end{aligned} \tag{1}$$

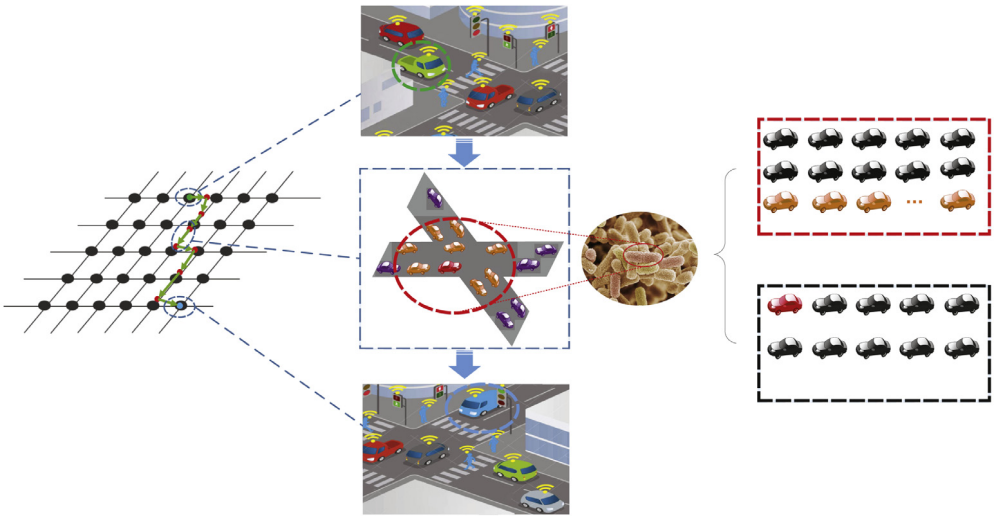

Fig. 1. The schematic diagram of MRVT-CAS.

(2) Construction of normalized decision matrix NDM_i.
In order to eliminate impact of measurement units of the four attributes, the data is normalized by Eq. (2). NDM_i is the normalized decision matrix. $attr = 1, 2, 3, 4$ represents four attributes. $c = 1, 2, \ldots, n$ represents vehicle in V_i. $x_{c,attr}$ is the element of DM_i at point $(c, attr)$. $y_{c,attr}$ is normalized value of $x_{c,attr}$.

$$y_{c,attr} = \frac{x_{c,attr}}{\sqrt{\sum_{c=1}^{n} x_{c,attr}^2}} \tag{2}$$

(3) Construction of weighted matrix decision matrix WDM_i.
Because the IoVs is highly dynamic, the above four attributes of each vehicle change fast, which is possible to cause statistical change of attributes. In order to eliminate influence of subjective weights on the method, entropy method is utilized to generate dynamic weight. The weight of each attribute ω_{attr} can be calculated by Eq. (3). H_{attr} is entropy of each attribute. $Noa = 4$ represents number of attributes. Then the element of WDM_i can be obtained by Eq. (4), $z_{c,attr}$ is weighted value of $y_{c,attr}$.

$$\begin{cases} f_{c,attr} = \dfrac{1 + y_{c,attr}}{\sum_{attr=1}^{Noa}(1 + y_{c,attr})} \\ H_{attr} = \dfrac{1}{-\ln(Noa)}\left(\sum_{attr=1}^{Noa} f_{c,attr} \ln f_{c,attr}\right) \\ \omega_{attr} = \dfrac{1 - H_{attr}}{Noa - \sum_{attr=1}^{Noa} H_{attr}} \end{cases} \tag{3}$$

$$z_{c,attr} = y_{c,attr} \cdot \omega_{attr} \tag{4}$$

(4) Calculation of the best solution and the worst solution
For each attribute, the best solution Z_{attr}^{+} and the worst solution Z_{attr}^{-} is established by Eq. (5). Then we can obtain the best solution vector $Z^{+} = \left[Z_1^{+}, Z_2^{+}, Z_3^{+}, Z_4^{+}\right]$, and the worst solution vector $Z^{-} = \left[Z_1^{-}, Z_2^{-}, Z_3^{-}, Z_4^{-}\right]$.

$$\begin{aligned} Z_{attr}^{+} &= \min_{c \in V_i}\left\{z_{c,attr}\right\} \\ Z_{attr}^{-} &= \max_{c \in V_i}\left\{z_{c,attr}\right\} \end{aligned} \tag{5}$$

(5) Generation of candidate set of next-hop node
For each vehicle c in WDM_i, Eq. (6) is used to calculate the euclidean distance S_c^{+} between the attributes vector of c and Z^{+}, and euclidean distance S_c^{-} between the attributes vector of c and Z^{-}. Then the score of each vehicle c is derived by Eq. (7). Finally, TN_{nv}(TN_{nv} is positive constant) vehicles with top TN_{nv} scores are selected to generate candidate set of next-hop node VC_i. Specially, VC_i is set equal to V_i if the number of vehicles in V_i is less than TN_{nv}.

$$\begin{aligned} S_c^{+} &= \sqrt{\sum_{attr=1}^{Noa}\left(z_{c,attr} - Z_{attr}^{+}\right)^2} \\ S_c^{-} &= \sqrt{\sum_{attr=1}^{Noa}\left(z_{c,attr} - Z_{attr}^{-}\right)^2} \end{aligned} \tag{6}$$

$$S_c = \frac{S_c^{-}}{S_c^{-} + S_c^{+}} \tag{7}$$

3.3. Next-hop node selection based on cellular attractor

After constructing candidate set VC_i, the next-hop node is selected in VC_i based on cellular attractor selection model (CASM). The set consisting of i and VC_i are regarded as a cell, and the activity of cell is α. The possibility of vehicle j in VC_i being selected is m_j, and the state that the vehicle j in VC_i is selected as next-hop node is regarded as a kind of cellular attractor, which represents concentration of a kind of mRNA. The time of current packet staying at i and the congestion of next-hop node j_i^{*} is used to evaluate performance of transmission from i to j_i^{*}. This performance is considered as environment changes of cell, which influences α and m_j in later routing. We use the above process to map the next-hop node selection of video transmission in IoVs into cellular attractor selection method. For current data packet in current node i, the process of selection and update is as follow.

(1) Calculating m_j of each j

(A) The demand node D is in the VC_i.
The possibility of D being selected is assigned as $m_D = 1$. However, the possibilities of other vehicles in VC_i cannot be assigned as $m_j = 0$ directly. That is because it will influence the process of selection of next-hop node in later routing. In order to avoid this influence, the m_j of other vehicles in VC_i is determined by Eq. (8).

$$m_j = \frac{1}{|VC_i| - 1} \tag{8}$$

(B) The demand node D is not in the VC_i.

(a) i is not one of nodes in previous routing paths. This situation represents that the cell including i and VC_i is not activated, and there is no information about corresponding α and m_j. So the possibility of all vehicles in VC_i is equal, and it is calculated by Eq. (9).

$$m_j = \frac{1}{|VC_i|} \tag{9}$$

(b) i is one of nodes in previous routing paths. Because the IoVs is highly dynamic, the neighbor vehicles VC_i of i in current routing path is possible different to neighbor vehicles PVC_i of i in precious routing paths. Eq. (10) is used to divide vehicles in VC_i into two sets.

$$\begin{aligned} VC_i' &= VC_i \cap PVC_i \\ VC_i'' &= VC_i - PVC_i \end{aligned} \tag{10}$$

For vehicles in VC_i'', they are not the neighbor vehicles of i in precious routing paths. Their m_j is determined by Eq. (11).

$$m_j = \frac{1}{|VC_i''|} \tag{11}$$

For vehicles in VC_i', they are the neighbor vehicles of i in precious routing paths, which represents that there are information of their selected possibility m_j' in precious routing paths. Their m_j in current routing paths can be calculated Eq. (12).

$$m_j = \frac{m_j'}{\sum_{k \in VC_i'} m_k} \times \left(1 - \frac{|VC_i''|}{|VC_i|}\right) \tag{12}$$

(2) Selecting the next-hop node j_i^*
Eq. (13) is utilized to select the next-hop vehicle node j_i^* with the maximum m_j. If m_j of several vehicles are maximum and equal, one vehicle in these vehicles is selected at random as j_i^*.

$$j_i^* = \arg\max \left\{ m_j | \forall j \in VC_i \right\} \tag{13}$$

(3) Updating α and m_j
The α and m_j of cell are updated after i selects the next-hop node j_i^* and finishes the transmission of current data packet from i to j_i^*. First, the performance index $PI_{ij_i^*}$ of this selection is calculated by Eq. (14).

$$PI_{ij_i^*} = \omega_t x_t + \omega_n x_n \tag{14}$$

where x_t is the time from i receiving current data packet to j_i^* receiving it, x_n is the numbers of data packets carried by j_i^*, ω_t and ω_n are corresponding weight coefficient. Then activity α can be updated by Eq. (15).

$$\alpha = \frac{A}{B + (PI_{ij_i^*})^{\kappa}} \tag{15}$$

where A, B, κ are positive constant. A, B are utilized to limit the boundaries of α, and κ is used to control the change rate of α.

In Fig. 2, we use the value of parameters in Table 3 to draw the functional image of α, which shows the impact of x_t and x_n. From Fig. 2, it can be found that α will decrease with the increases of x_t and x_n, and functional image of α can be divided into three parts: slowly descend part, sharply descend part and convergence part. In slowly descend part, the increases of x_t and x_n are possible resulted from that multiple video resource nodes are sending data packets simultaneously, and these data packets can be forwarded to other nodes in short time. Therefore, this decrease of α can be tolerable and be independent of cell performance. In order not to influence later transmission process, the descent speed of α is set to be slow in this part. In sharply descend part, there are unacceptable increases of x_t and x_n, which is probably caused by the improper selection of next-hop node and will result in a degree of delay of transmission. For the sake of punishing this cell, the α of cell in this part is set to decrease sharply. In convergence part, the x_t and x_n are so large that it will lead to serious delay, which will affect the efficiency and quality of video transmission badly. Thus the α of cell in this part tends to 0 to avoid that these cells are selected in later transmission.

Last, m_j can be updated by Eq. (16).

$$m_j = m_j' + \left(\frac{s(\alpha)}{1 + (m_{j_i^*} - m_j)^2} - d(\alpha) m_j + \eta_j\right) \times \Delta t \tag{16}$$

Δt is V2V communication delay, which is the time from i sending out packet to j_i^* receiving this packet. $s(\alpha)$ is the rate coefficient of producing the cellular activity, and $s(\alpha)$ is the rate coefficient of degradation. The two functions are both effected by the cellular activity, and they are defined by Eq. (17).

$$\begin{cases} s(\alpha) = \lambda_1 \alpha^r + \lambda_2 \alpha \\ d(\alpha) = \alpha \end{cases} \tag{17}$$

where λ_1, λ_2 and r are real-number constants.

3.4. Routing procedure

Based on the models and algorithms in Section 3, we show the routing procedure of MRVT-CAS in Fig. 3.

4. Performance evaluation

In Section 4, we give the performance evaluation based on some comparative simulations. These simulations are achieved in MATLAB with SUMO traffic simulator. We compare video transmission performance of MRVT-CAS with URAS and GPSR. Through these simulations under different conditions, we validate that MRVT-CAS has better performance in video transmission.

4.1. Simulation scenario and basic model settings

In the simulations, a bi-direction and four lane road which is 8000 m long is considered. The average vehicle speed $\bar{v}$ is varying from 10 m/s to 37.5 m/s, and the vehicle density K is varying from 10 veh/km/lane to 120 veh/km/lane. The different $\bar{v}$ and K represent different traffic conditions, including free-flow, unimpeded, crowded and blocked. The speed of vehicles subjects to normal distribution with mean $\bar{v}$ and standard deviation $\sigma_v = 0.1 * \bar{v}$, and the upper bound of speed is limited to $2 * \bar{v}$. And for fleets, they are traveling based on Wiedemann car-following model.

In addition, simulation time is 25 s, and total steps of simulation are 2500, and each vehicle only can forward one packet in a step. The communication range of each vehicle is 300 m, and the vehicle-to-vehicle (V2V) communication delay is 10 ms. In order to ensure the real-time of transmission, we set the survival limit of the data packets to 5 s, which means the data packets with the existence time in simulation more than 5 s will be abandoned. The initial distance between resource node and demand node is 1200 m, and this distance will change with the motion of resource node and demand node. We use three pairs of resource–demand nodes communicating simultaneously to consider the influence of multiple communication links. Each resource node sends 100 data

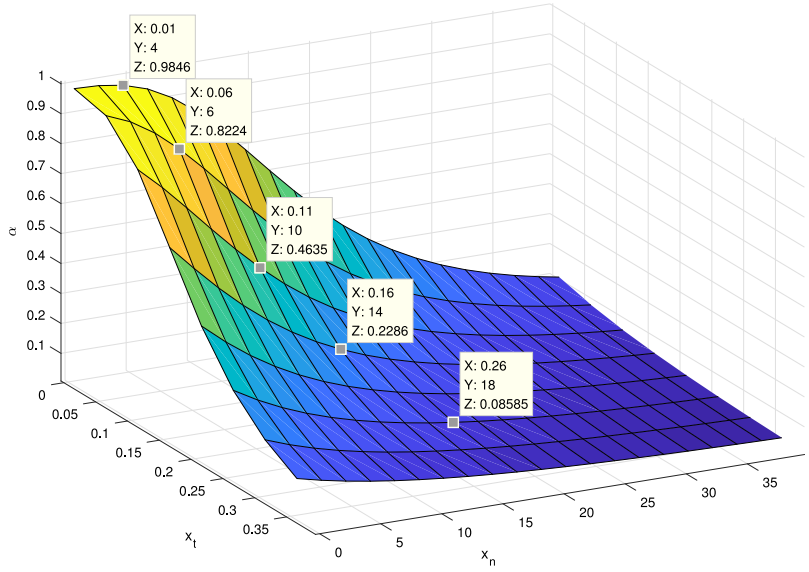

Fig. 2. The impact of x_t and x_n on α.

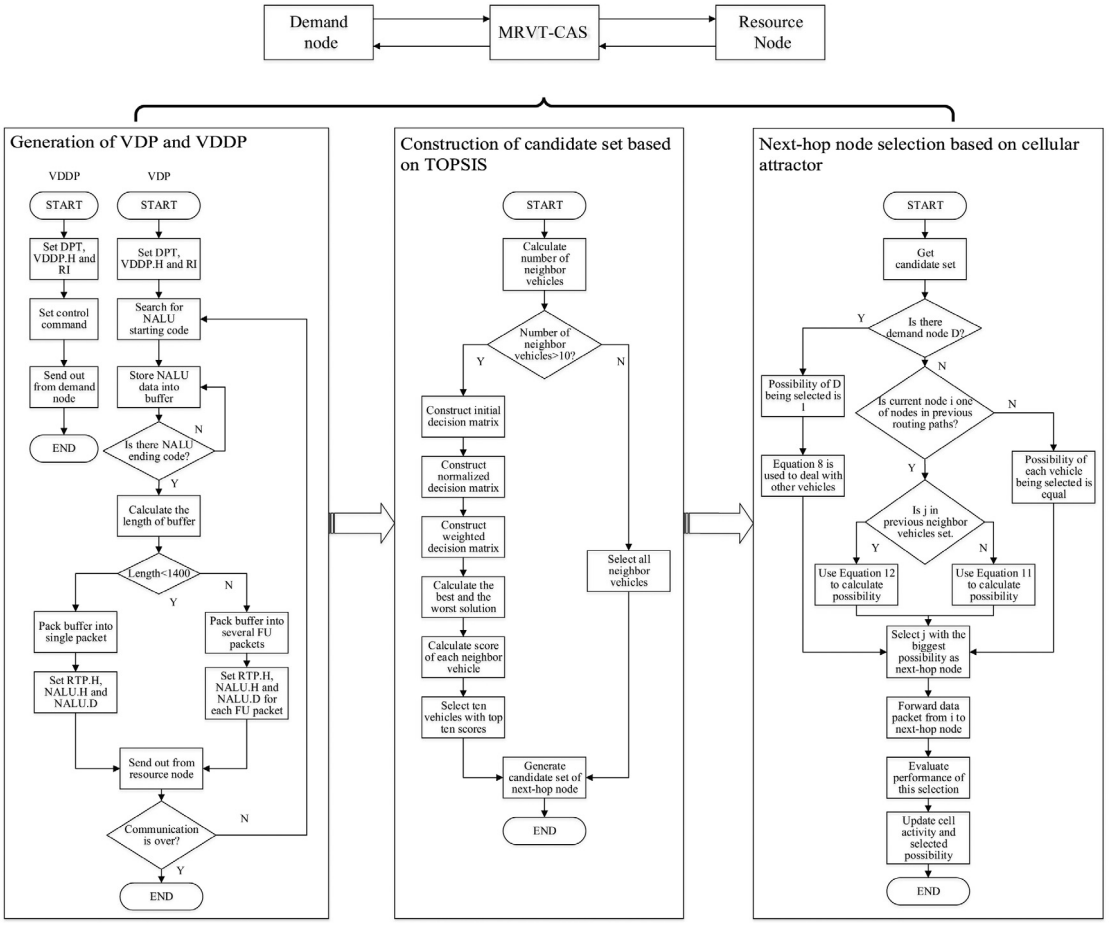

Fig. 3. Routing procedure of MRVT-CAS.

packets per second in first 20 s of 25 s, so each resource node sends total 2000 data packets in each simulation.

For video frames, we set the Group of Pictures (GOP) pattern as "IPPP", and each I frame occupying two data packets while each P frame occupying one data packet. The buffer time of video frame is 0.1 s, which means demand node will abandon the $No.(n+1)$ data packets if the arrival time of $No.(n+1)$ is more than 0.1 s later than that of $No.(n)$ ($No.(n)$ and $No.(n+1)$ are in original sequence of frames). What is more, the demand will abandon all data packets of the GOP whose data packets corresponding to the I frame is missing. We use this situation of transmitting hundreds data packets with different types of frames per second to simulate

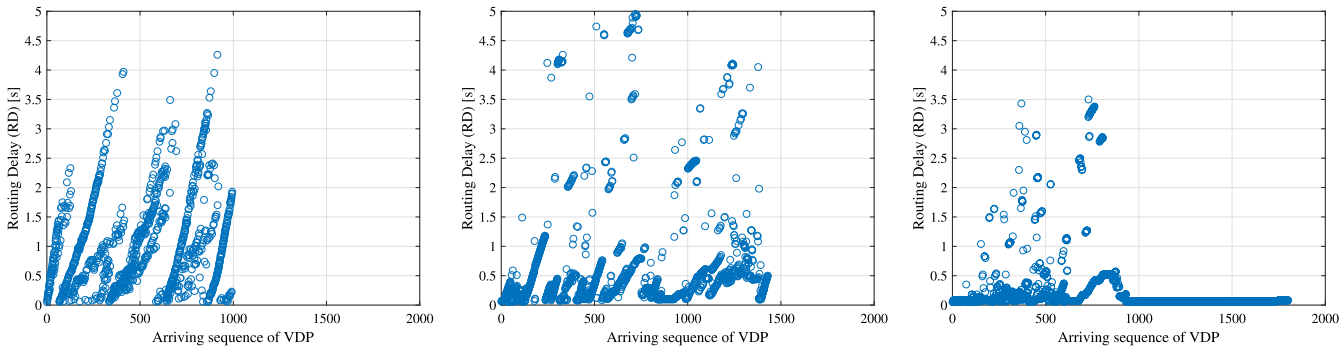

Fig. 4. The results of DPDR and RD for the second pair resource–demand node.

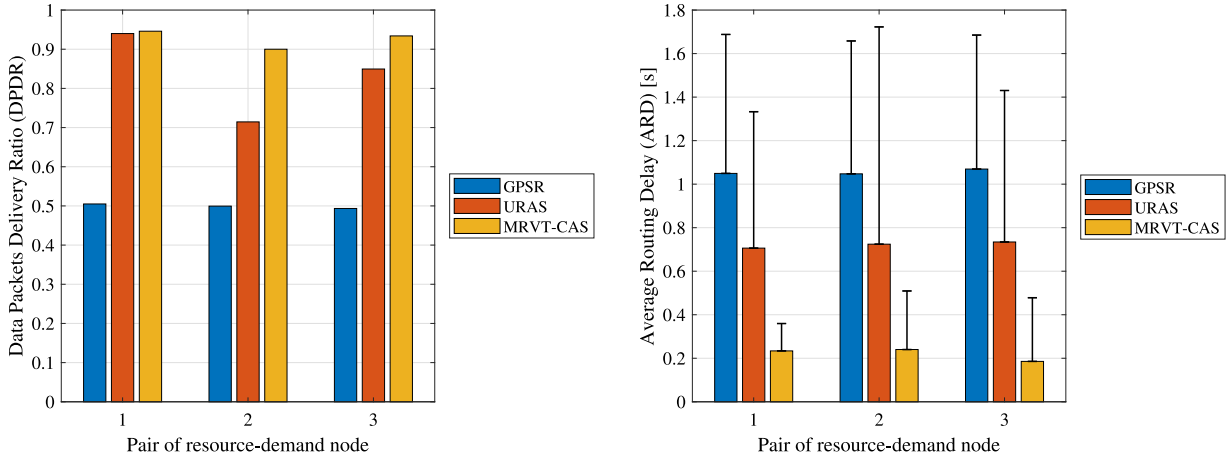

Fig. 5. The results of DPDR and ARD for three pairs resource–demand node.

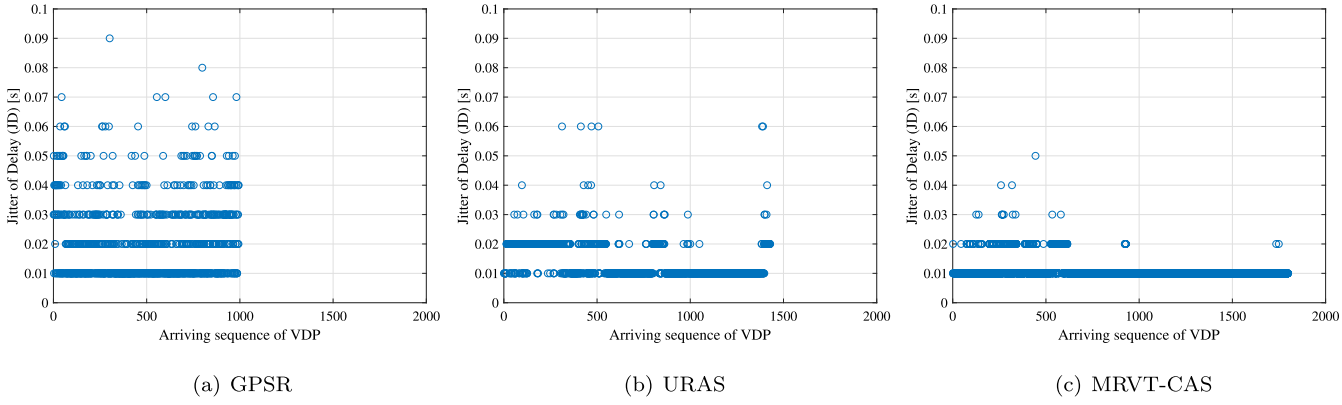

Fig. 6. The results of JD for the second pair resource–demand node.

video transmission in IoVs. The other basic model settings for simulations are given in Table 3.

4.2. Simulation results and analysis

The simulation experiments are conducted for comparing three routing protocols in VANETs: the proposed MRVT-CAS, the URAS proposed in early work [19] and GPSR [32]. In order to comparatively demonstrate the validation of MAVT-CAS as well as confirm its strength in terms of the comprehensive performance on the transmission efficiency and quality, the following performance indexes are adopted for the comparative evaluation of these three routing protocols:

Table 3
Basic model settings.

Parameters	Values
ω_t, ω_n in Eq. (14)	$\omega_t = 5, \omega_n = 0.05$
A, B and κ in Eq. (15)	$A = 1, B = 1$ and $\kappa = 5$
Δt in Eq. (16)	$\Delta t = 0.01$
λ_1, λ_2 and r in Eq. (17)	$\lambda_1 = 8, \lambda_2 = 10$ and $r = 4$

(1) The Data Packets Delivery Ratio (DPDR) that is measured as the ratio of the number of data packets arriving at the demand node to the number of data packets sent by resource node.
(2) The Average Routing Delay (ARD) that is defined as the average time from the resource node to demand node among all the complete resource–demand routing paths.
(3) The Jitter of Delay (JD) that is computed by differencing the delay of two adjacent data packets arriving at the demand node.
(4) The Out-of-order Data Packets Loss Ratio (ODPLR) that is defined as ratio of number of data packets is abandoned because of arriving out-of-order to the amount of data packets arriving at the demand node.
(5) Video Frame Transmitted Successfully Ratio (VFTSR) that is measured as the rate of the number of frames transmitted successfully to the amount of frames sent by resource nodes. According to the type of frame, the loss of frames can be divided into two situations: (1) If data packet of P frame is lost, it causes only one P frame is lost. (2) If data packet of I frame is lost, it causes the corresponding GOP is abandoned, which means demand node will lose four frames in this GOP.

4.2.1. Evaluation under specific condition

Firstly, we will describe the evaluation under specific condition and give some microcosmic results. We set the vehicle density to 80 veh/km/lane and the vehicle speed to 20 m/s. The thresholds of the number of neighbor vehicles TN_{nv} is set to 10. In the following analysis, the second pair of resource–demand node is taken as an example to show concrete results of each routing path. In addition, we give the statistical values of all three pairs.

From Fig. 4, it can be found that the DPDR of MRVT-CAS is larger than GPSR and URAS, in addition, ARD of MRVT-CAS is less than GPSR and URAS. We can intuitively see that MRVT-CAS can receive around 1800 data packets, while that of URAS is 1400, and that of GPSR is only 1000. For ARD, it can be found that the delays of data packets of MRVT-CAS are in 0.1 s–0.5 s interval, while those of URAS are in 0.3 s–1 s, and those of GPSR are distributed in 0.1 s–4 s. Besides, there are regular ups and downs of ARD in Fig. 4(a). That is because GPSR always selects the closest node to demand node in communication range, and this closest node is possible changeless in short time. So it causes this closest node accumulate many data packets, and the delays of the later data packets increase linearly. Until some packets reach survival limit 5 s or the closest node changes, this congestion can be relieved, and the delays of the later data packets will decrease linearly. In addition, there are also slight ups and downs of ARD in Fig. 4(b). Because when there is congestion in some nodes, the selected possibilities of these node are updated until data packets passing through these nodes arrive demand node. This delay of information updated causes that many nodes in congestion still be selected, which results in more serious congestion and delay. On the contrary, there are few ups and downs of ARD in Fig. 4(c). That is because that we take into consideration several motion and communication parameters by combining TOPSIS and the entropy method. When some nodes are in congestion, their scores determined by TOPSIS are low, and they cannot be selected into candidate set. After the current data packet is forwarded to next-hop node from node in congestion, the cell activity of the node is updated immediately. This real-time feedback process not only eases congestion but reduces the influence of congestion on the later data packets.

In Fig. 5(a), we give the statistic results of DPDR among three pairs of resource–demand node. In this simulation, our proposed MRVT-CAS achieves about 94.0% of DPDR on average, which is larger than those of GPSR (49.9%) and URAS (about 83.5%). Fig. 5(b) shows the ARD results achieved by GPSR, URAS and MRVT-CAS, in addition, the length of error bars is used to present the standard deviation of ARD. As shown in 5(b), MRVT-CAS achieves 0.219 s on average among three pairs of resource–demand nodes, which is less than those of GPSR (about 1.055 s) and URAS (0.861 s). The similar conclusion can also be drawn that MRVT-CAS achieves less standard deviation (about 0.228 s), while that of GPSR is 0.773 s and that of URAS is 0.621 s. The results of DPDR and ARD show that MRVT-CAS has better reachability performance in condition of multiple communication links, and it can guarantee the delivery rate while minimizing the time cost.

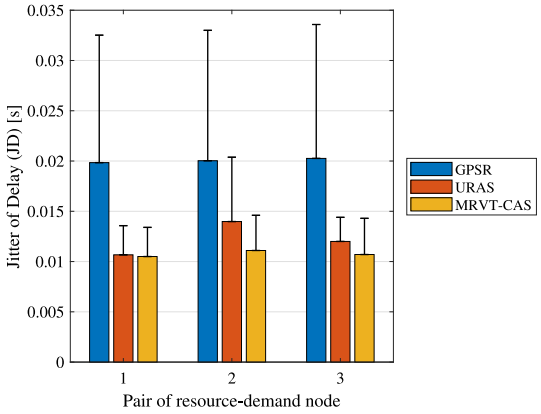

Fig. 7. The results of JD for three pairs resource–demand node.

Jitter of Delay (JD) is a vital important stability index of communication in IoVs, and the large JD causes that the information received by demand node is intermittent. Fig. 6 shows the JD of every two adjacent data packets arriving at the demand node in the second pair of resource–demand nodes. It can be found that JD of MRVT-CAS is obviously less than that of GPSR and URAS. Fig. 7 shows the statistical results of JD achieved by above three routing protocols. We can see that MRVT-CAS achieves about 0.0107 s of JD on average, while that of GPSR is 0.0202 s and that of URAS is 0.0122 s. The results show that MRVT-CAS has better stability than GPSR and URAS.

Because IoVs is a fast changing topology, the arrival order of data packets is usually not the same as original order. This phenomenon influences decode process of demand node and affects the quality of video transmission in IoVs. The data packets whose arrival order is later than original order are regarded as "out-of-order data packet". As mentioned in Section 4.1, demand node will abandon the $No.(n+1)$ data packet if the arrival time of $No.(n+1)$ is more than 0.1 s later than that of $No.(n)$ ($No.(n)$ and $No.(n+1)$ are in original sequence of frames). According to the results in Fig. 6, it can be found that the maximum of JD is not more than 0.1 s, so these abandoned data packets are all "out-of-order data packet". In this simulation, arriving time and ODPLR are used to evaluate the performance of avoiding disorder of data packets. In Fig. 8, x-axis is the original sequence of VDP, and y-axis is their arriving time. It can be found that the result of MRVT-CAS is more fitted by a straight line than those of GPSR and URAS, which shows MRVT-CAS has better performance of keeping sequentially of data packets intuitively. Fig. 9 illustrates that MRVT-CAS loses 4.1% of received data packets because of out-of-order arriving order, which is less than that of GPSR (about 31.5%) and that of URAS (about 7.5%). As shown in analysis of DPDR, the low reachability performance of routing protocols results in loss of data packets, and these data packets are set as the set LDP_1. As shown in analysis of ODPLR, the out-of-order sequence also results in loss of data packets, and these data packets are set as the set LDP_2. Original data packets of each resource node is set as IDP, then the remainder data packages provided to the decoder of demand node is $REDP = IDP - LDP_1 - LDP_2$.

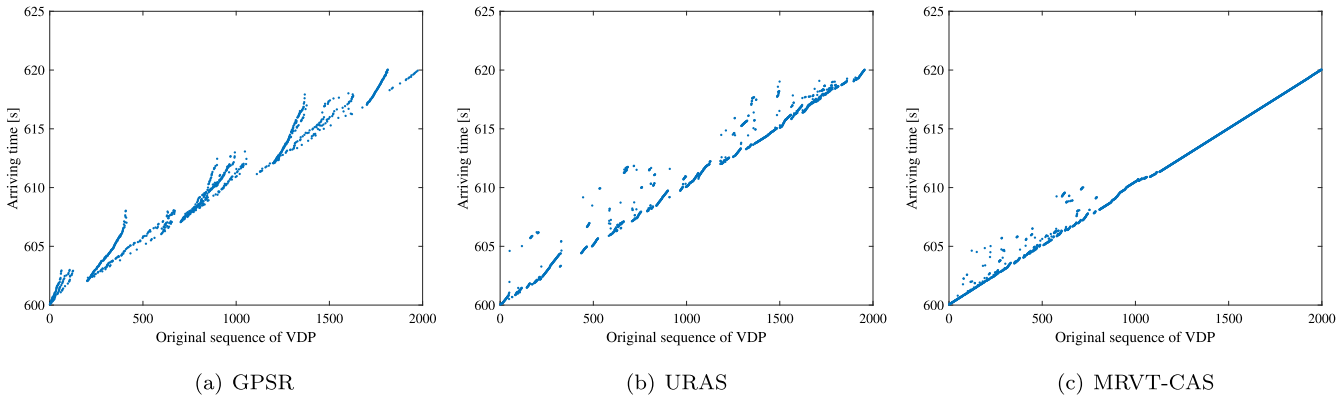

Fig. 8. The results of arriving time for the second pair resource–demand node.

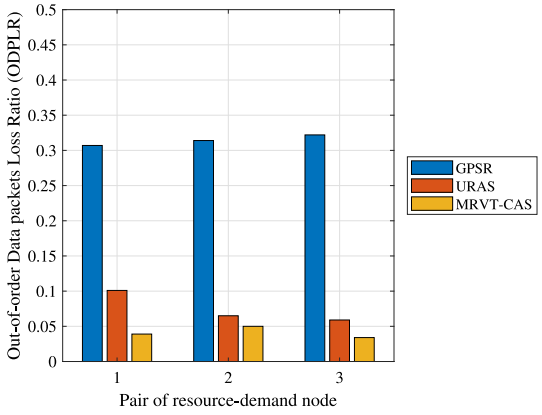

Fig. 9. The results of ODPLR for three pairs resource–demand node.

The loss of data packets results in the loss of video frames related to LDP_1 and LDP_2. Based on the hypothesis of simulation, if the data packet of the P frame is lost, it only affects the P frame, but it affects the whole GOP if the data packets of I frame are lost. Fig. 10 shows the results of VFTSR achieved by MRVT-CAS, URAS and GPSR, which evaluate the influence of different routing protocols on decoded video frames. In Fig. 10, the blue part represents the percentage of I frame, the orange red part represents the percentage of P frame, and the line $y = 0.25$ represents the initial proportion of I frame in video stream. It can be found that the VFTSR result of MRVT-CAS is about 80.7%, including 21.0% I frame and 59.7% P frame. The VFTSR result of URAS is 67.4%, including 17.8% I frame and 49.6% P frame. The VFTSR result of GPSR is 13.1%, including 4.7% I frame and 8.4% P frame. The results of VFTSR illustrate that MRVT-CAS has better performance of restoring video stream in this simulation than URAS and GPSR.

4.2.2. Evaluation under different thresholds of the number of vehicle in candidate set

In order to research influence of difference thresholds of the number of vehicle in candidate set TN_{nv} to performance of MRVT-CAS, we set TN_{nv} to vary from 1 to the number of neighbor vehicles $|V_i|$ (the average value is about 95). Here, the vehicle density is 80 veh/km/lane and the vehicle speed is 20 m/s.

Fig. 11 shows the changing of α when TN_{nv} is 3, 10, 50 and $|V_i|$. We can intuitively see that TN_{nv} significantly affects the cell activity α. Additionally, we select ten values of TN_{nv}(1, 3, 7, 10, 20, 35, 50, 65, 80, $|V_i|$) to show statistical results of influence of TN_{nv} to cell activity α and MRVT-CAS performance.

Fig. 12 shows the results of average cell activity under different TN_{nv}. It can be found that average cell activity is low when TN_{nv} is in interval [1, 7]. Especially, MRVT-CAS achieves only 0.29 of average cell activity when TN_{nv} is 1. That is because the nodes offered to the process of next-hop selection based on cell attractor selection are too little when TN_{nv} is vital small, which weakens the performance of the CASM in MRVT-CAS. On the contrary, MRVT-CAS can achieve 0.93 of average cell activity over the interval [10, 35]. That is because TOPSIS and CASM can work well collaboratively under this condition. TOPSIS selects proper number of vehicles to construct VC_i and CASM selects the next-hop node with high performance in VC_i. Moreover, increasing TN_{nv} leads to decreasing average cell activity in the interval [35, $|V_i|$]. Especially, MRVT-CAS achieves only 0.58 of average cell activity when TN_{nv} is $|V_i|$, which results form that TOPSIS cannot play a role under this condition.

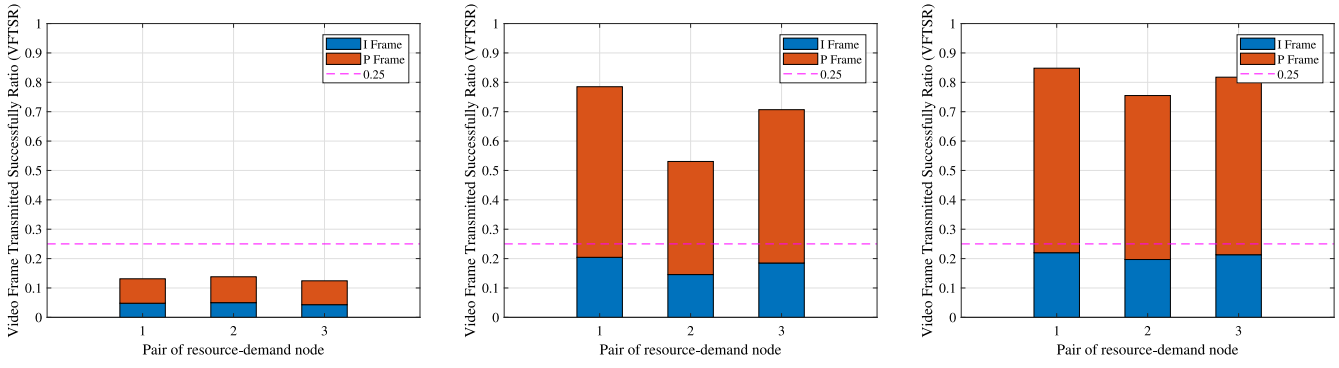

Fig. 10. The results of VFTSR for three pairs resource–demand node.

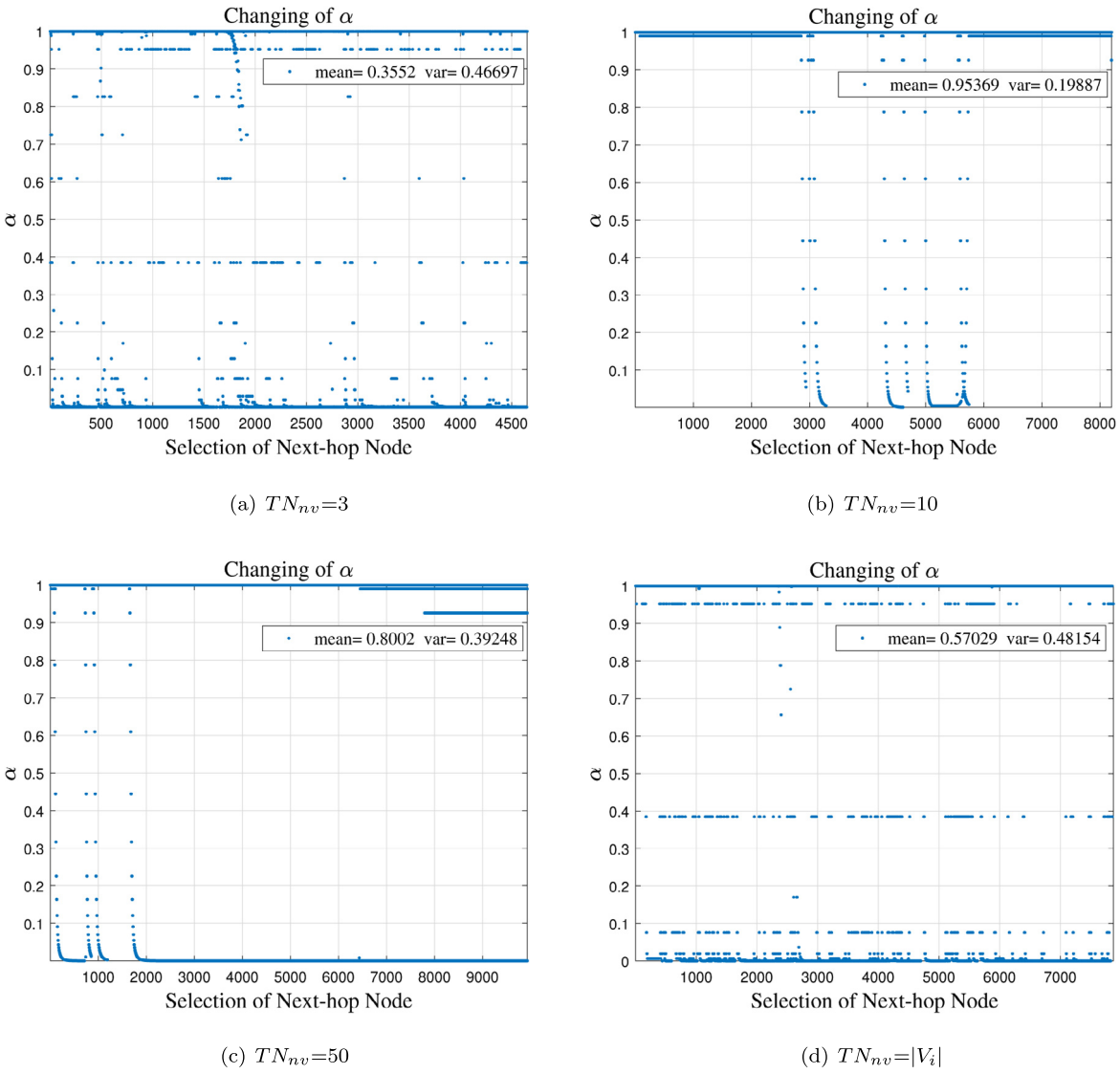

Fig. 11. The changing of α under different TN_{nv}.

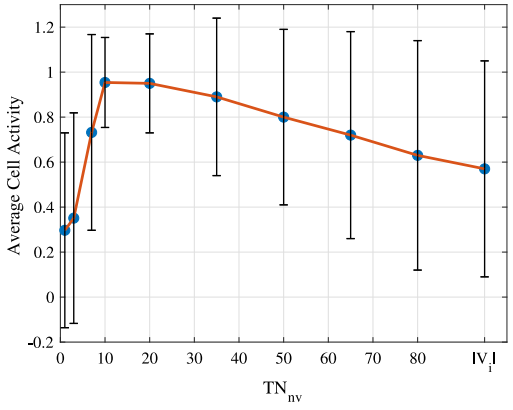

Fig. 12. The average cell activity under different TN_{nv}.

Fig. 13 shows the video transmission performance of MRVT-CAS under different TN_{nv}. From Figs. 13(a) and 13(b), it can be found that the increasing TN_{nv} in the interval [1, 10] leads to increasing of DPDR and decreasing of ARD, which results from that too small TN_{nv} brings about inoperative of CASM in MRVT-CAS, but with the increasing of TN_{nv}, more nodes in high performance selected by TOPSIS can be offered to CASM, and the real-time feedback based on CASM guarantees the reachability and low delay of MRVT-CAS. On the contrary, increasing TN_{nv} in the interval [20, $|V_i|$] leads to decreasing of DPDR and increasing of ARD. That is because TOPSIS is ineffective when TN_{nv} is too large, which causes that the next-hop node selected by CASM may not have good motion and communication performance.

From Fig. 12, the standard deviation of cell activity is large when TN_{nv} is very small and very large, which means there is a lot of randomness in selection of next-hop node under these conditions. Additionally, this randomness leads to great instability in video transmission. As shown in Fig. 13(c), MRVT-CAS achieves 0.0280 s of JD when TN_{nv} is 1 and 0.0245 s of JD when TN_{nv} is $|V_i|$, while JD is only 0.0107 s when TN_{nv} is 10. Moreover, this randomness also results in that some data packets are lost because of out-of-order arriving order. As shown in Fig. 13(d), MRVT-CAS loses 28.27% of received data packets when TN_{nv} is 1 and 13.60% when TN_{nv} is $|V_i|$, while ODPLR is only 4.10% when TN_{nv} is 10.

Fig. 13(e) shows the results of VFTSR under different TN_{nv}, it

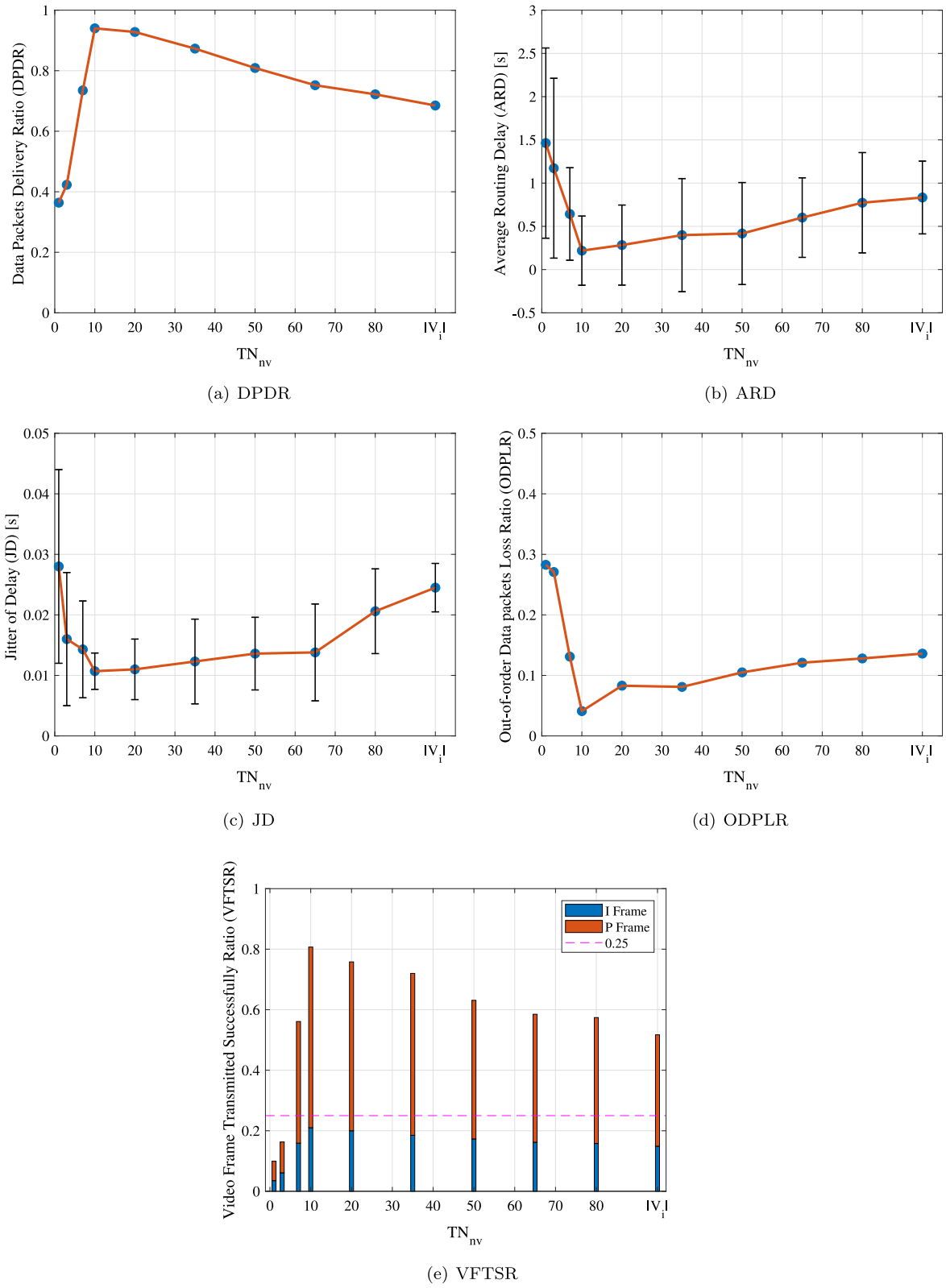

Fig. 13. The video transmission performance of MRVT-CAS under different TN_{nv}.

can be found that TN_{nv} greatly affects the quality of video received by demand node. Over the interval [1, 3], MRVT-CAS only achieves 13.1% of VFTSR on average. Additionally, MRVT-CAS achieves 57.6% of VFTSR within [50, $|V_i|$]. On the contrary, MRVT-CAS can obtain 73.2% of VFTSR in [10, 50).

4.2.3. Evaluation under different traffic conditions

In order to evaluate performance of MRVT-CAS in difference traffic conditions, we take into consideration several different traffic flows. Here, the threshold of the number of vehicle in candidate set TN_{nv} is 10. The average vehicle speed $\bar{v}$ and the vehicle density

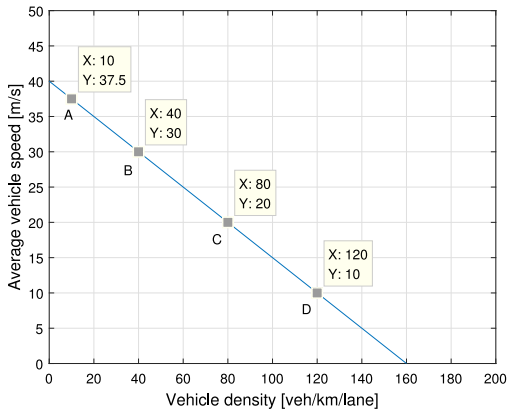

Fig. 14. The diagram of $\bar{v}$ and K.

K are determined by Greenshields [33] model in Fig. 14, and the model is shown as Eq. (18).

$$\bar{v} = 40 * (1 - \frac{K}{160}) \tag{18}$$

In the following analysis, we select four kinds of traffic flows in Fig. 14 to evaluate performance of GPSR, URAS and MRVT-CAS.

The results of DPDR and ARD are shown in Fig. 15. We can find the increasing vehicle density leads to increasing DPDR and decreasing of GPSR, URAS and MRVT-CAS, which represents that a traffic network with a large density can better guarantee the reachability of routing protocols. That is because that large vehicle density enables more nodes with high performance can be selected, on the contrary, small vehicle density may cause all candidate nodes are in congestion. Moreover, the DPDR results of MRVT-CAS under these four traffic conditions are all better than those of GPSR and URAS. Specially, when vehicle density is 10 veh/km/lane, the advantage of MRVT-CAS relative to GPRS and URAS is vital obvious. Under this traffic condition, MRVT-CAS can achieve 81.2% of DPDR while that of URAS is 53.9% and that of GPSR is only 32.5%. GPSR always selects the closest node to demand node in communication range, and this closest node is possible changeless in long time when vehicle density is very low. This phenomenon results in serious congestion in some nodes, and massive packets cannot be transmitted within survival limit. For URAS, it achieves 2.1 s of ARD under this traffic condition, which represents the possibilities of the nodes in current routing path are updated about two seconds after current routing path starting.

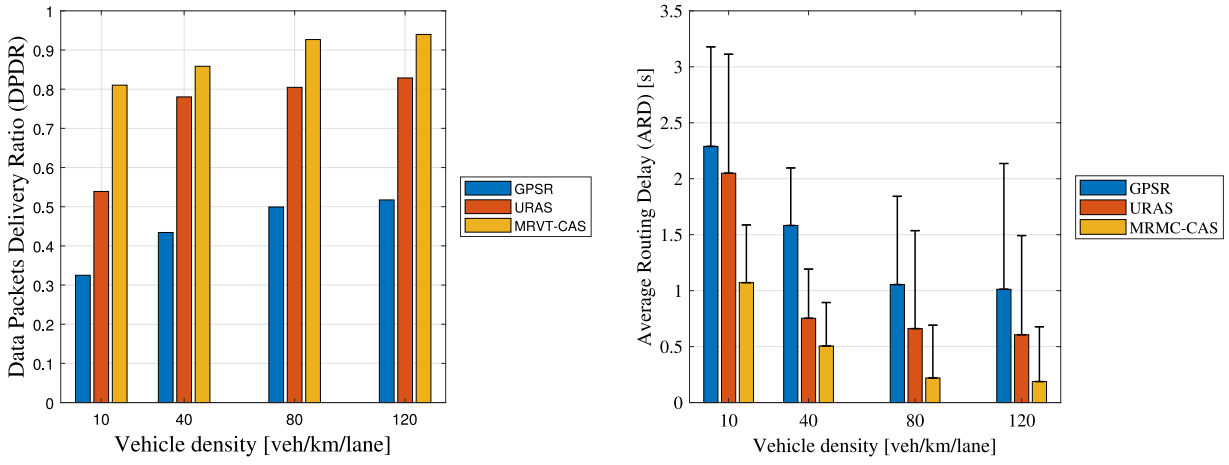

(a) DPDR (b) ARD

Fig. 15. The results of DPDR and ARD under different traffic conditions.

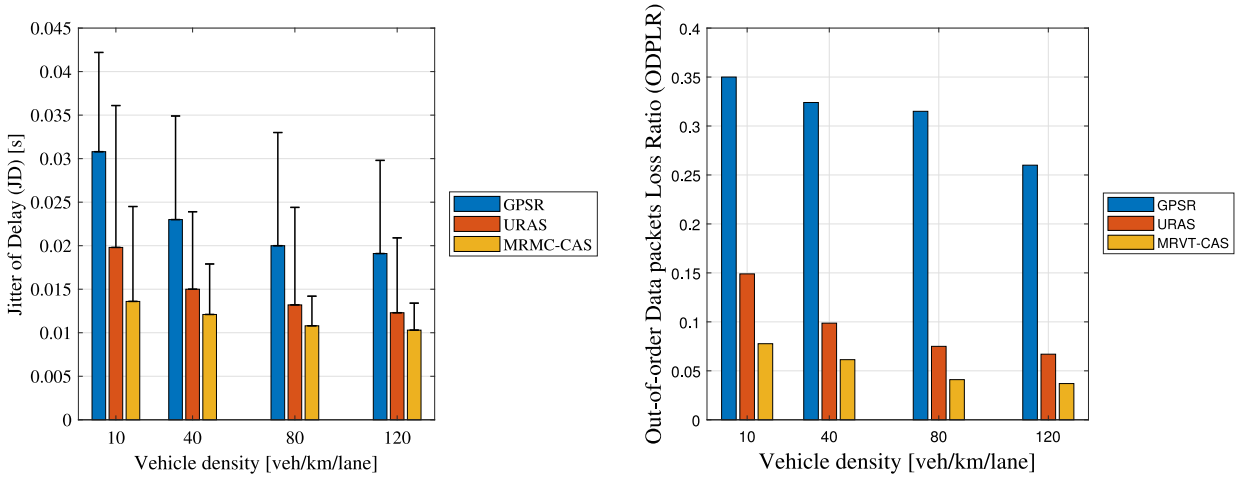

(a) JD (b) ODPLR

Fig. 16. The results of JD and ODPLR under different traffic conditions.

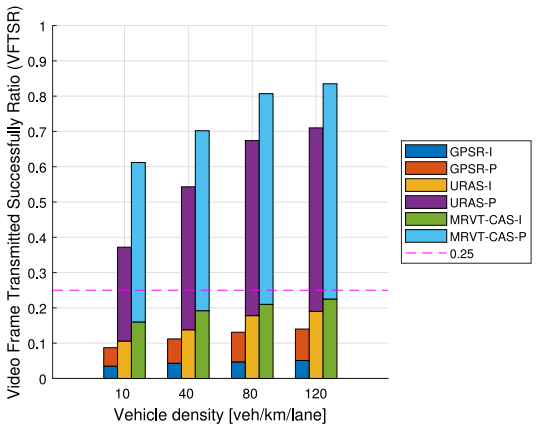

Fig. 17. The results of VFTSR under different traffic conditions.

This delay results in improper selection of next-hop node and exacerbates the congestion of some nodes with low performance, which causes low reachability performance of URAS finally.

The results of JD and ODPLR are shown in Fig. 16. It can be found that the increasing vehicle density leads to decreasing JD and ODPLR, which represents that the dense traffic flow can improve stability of GPSR, URAS and MRVT-CAS. Additionally, over the interval [10,120](veh/km/lane), our proposed MRVT-CAS achieves 0.012 s of JD on average, which is smaller than those of URAS (about 0.015 s) and GPSR (about 0.023 s). Moreover, MRVT-CAS also obtains the lowest ODPLR that is 5.1% on average, while that of URAS is 10.9% and that of GPSR is 29.1%.

In Fig. 17, we give the results of VFTSR achieved under different traffic conditions. It can be found that the traffic condition significantly affects the performance of these routing protocols. The results in Fig. 17 imply that a denser traffic network potentially decreases the frame loss rate of GPSR, URAS and MRVT-CAS. Moreover, over the interval [10,120](veh/km/lane), our proposed MRVT-CAS achieves 73.9% of VFTSR on average (including 19.6% I frame and 54.3% P frame), which is larger than those of URAS (about 57.5%, including 15.3% I frame and 42.2% P frame) and GPSR (about 11.8%, including 4.4% I frame and 7.4% P frame). Especially, even under a high mobility traffic network (vehicle density is 10 veh/km/lane and average vehicle speed is 37.5m/s), MRVT-CAS also can achieve 61.2% of VFTSR, while that of URAS is 37.2% and that of GPSR is 8.7%. This advantage of frame loss rate benefits from the real-time feedback based on cell attractor selection, which can make full use of current VANET resources, and assign tasks of data packets transmitting to nodes in current VANET reasonably and efficiently.

5. Conclusion

In this paper, we have proposed a multi-hop routing protocol for video transmission in IoVs based on cellular attractor selection, which is named as MRVT-CAS. First, we design a method of video data packets generation. Then we combine TOPSIS with entropy weight method to construct candidate set of next-hop node selection. Third, we use CASM to select next-hop node in candidate set. Specifically, we present a real-time feedback method based on performance of next-hop selection process to enhance MAVT-CAS's self-adaptability and robustness for video transmission in IoVs. Finally, our comparative simulation results have demonstrated that MRVT-CAS has better performance for video transmission in IoVs than GPSR and our previously proposed URAS in terms of reachability, delay, stability and frame loss rate.

Acknowledgments

This research was supported in part by the National Natural Science Foundation of China under Grant Nos. 61672082 and 61822101, Beijing Municipal Natural Science Foundation, China Nos. 4181002, Beihang University, China Innovation & Practice Fund for Graduate (Project NO. YCSJ-02-2018-05), Asa Briggs Visiting Fellowship from University of Sussex, UK, Royal Society-Newton Mobility Grant (IE160920) and The Engineering, and Physical Sciences Research Council (EPSRC), UK (EP/P025862/1).

References

[1] M. Chen, Y. Tian, G. Fortino, J. Zhang, I. Humar, Cognitive internet of vehicles, Comput. Commun. 120 (2018) 58–70, http://dx.doi.org/10.1016/j.comcom.2018.02.006.
[2] H. Hartenstein, K.P. Laberteaux, A tutorial survey on vehicular ad hoc networks, IEEE Commun. Mag. 6 (6) (2008) 164–171, http://dx.doi.org/10.1109/MCOM.2008.4539481.
[3] Y. Toor, P. Muhlethaler, A. Laouiti, Vehicle ad hoc networks: applications and related technical issues, Commun. Surv. Tutor. IEEE 10 (3) (2008) 74–88, http://dx.doi.org/10.1109/COMST.2008.4625806.
[4] E. Hossain, G. Chow, V.C.M. Leung, R.D. Mcleod, J. Mišić, V.W.S. Wong, O. Yang, Vehicular telematics over heterogeneous wireless networks: A survey, Comput. Commun. 33 (7) (2010) 775–793, http://dx.doi.org/10.1016/j.comcom.2009.12.010.
[5] M. Chen, Y. Miao, Y. Hao, H. Kai, Narrow band internet of things, IEEE Access 5 (2017) 20557–20577, http://dx.doi.org/10.1109/ACCESS.2017.2751586.
[6] A. Aliyu, A.H. Abdullah, O. Kaiwartya, Y. Cao, J. Lloret, N. Aslam, U.M. Joda, Towards video streaming in iot environments: Vehicular communication perspective, Comput. Commun. (2017) http://dx.doi.org/10.1016/j.comcom.2017.10.003.
[7] Y. Tian, M. Chen, L. Sousa, Ubiquitous multimedia: Emerging research on multimedia computing, IEEE Multimedia 23 (2) (2016) 12–15, http://dx.doi.org/10.1109/MMUL.2016.28.
[8] A. Torres, C.T. Calafate, J.C. Cano, P. Manzoni, Y. Ji, Evaluation of flooding schemes for real-time video transmission in vanets, Ad Hoc Netw. 24 (PB) (2015) 3–20, http://dx.doi.org/10.1016/j.adhoc.2014.07.030.
[9] D. Roy, M. Chatterjee, E. Pasiliao, Video quality assessment for inter-vehicular streaming with ieee 802.11p, lte, and lte direct networks over fading channels, Comput. Commun. (2017) http://dx.doi.org/10.1016/j.comcom.2017.09.010.
[10] M. Chen, Y. Qian, Y. Hao, Y. Li, J. Song, Data-driven computing and caching in 5g networks: Architecture and delay analysis, IEEE Wirel. Commun. 25 (1) (2018) 70–75, http://dx.doi.org/10.1109/MWC.2018.1700216.
[11] Y. Zhang, M. Chen, N. Guizani, D. Wu, V.C.M. Leung, Sovcan: Safety-oriented vehicular controller area network, IEEE Commun. Mag. 55 (8) (2017) 94–99, http://dx.doi.org/10.1109/MCOM.2017.1601185.
[12] K. Fall, S. Farrell, Dtn: an architectural retrospective, IEEE J. Sel. Areas Commun. 26 (5) (2008) 828–836, http://dx.doi.org/10.1109/JSAC.2008.080609.
[13] M. Chen, Y. Hao, M. Qiu, J. Song, W. Di, H. Iztok, Mobility-aware caching and computation offloading in 5g ultra-dense cellular networks, Sensors 16 (7) (2016) 974, http://dx.doi.org/10.3390/s16070974.
[14] P.T.A. Quang, K. Piamrat, K.D. Singh, C. Viho, Video streaming over ad-hoc networks: a qoe-based optimal routing solution, IEEE Trans. Veh. Technol. PP (99) (2016) 1–1, http://dx.doi.org/10.1109/TVT.2016.2552041.
[15] A. Kashiwagi, I. Urabe, K. Kaneko, T. Yomo, Adaptive response of a gene network to environmental changes by attractor selection, PLoS One 1 (1) (2006) e49, http://dx.doi.org/10.1371/journal.pone.0000049.
[16] D. Tian, J. Zhou, Y. Wang, Y. Lu, H. Xia, Z. Yi, A dynamic and self-adaptive network selection method for multimode communications in heterogeneous vehicular telematics, IEEE Trans. Intell. Transp. Syst. 16 (6) (2015) 3033–3049, http://dx.doi.org/10.1109/TITS.2015.2422144.
[17] D. Tian, J. Zhou, Z. Sheng, Y. Wang, J. Ma, From cellular attractor selection to adaptive signal control for traffic networks, Sci. Rep. 6 (2016) 23048, http://dx.doi.org/10.1038/srep23048.
[18] D. Tian, J. Zhou, Y. Wang, G. Zhang, H. Xia, An adaptive vehicular epidemic routing method based on attractor selection model, Ad Hoc Netw. 36 (P2) (2016) 465–481, http://dx.doi.org/10.1016/j.adhoc.2015.05.018.
[19] D. Tian, K. Zheng, J. Zhou, X. Duan, Y. Wang, Z. Sheng, Q. Ni, A microbial inspired routing protocol for vanets, IEEE Internet of Things J. PP (99) (2017) 1–1. http://dx.doi.org/10.1109/JIOT.2017.2737466.
[20] A.E. Luthra, Special issue on the h.264/avc video coding standard, IEEE Trans. Circuits Syst. Video Technol. (2003).
[21] V. Jacobson, R. Frederick, S. Casner, H. Schulzrinne, Rtp: A transport protocol for real-time applications, Ietf Rfc 2 (2) (2003) 459–482.
[22] D.B. Johnson, D.A. Maltz, J. Broch, Dsr: the dynamic source routing protocol for multihop wireless ad hoc networks, Ad Hoc Netw. 5 (2001) 139–172.
[23] M. Mohsen, K. Xu, C. Liu, L. Shen, Design and implementation of multi-hop video transmission experiment system in vanet, J. Southeast Univ. (English Edition) (2014) http://dx.doi.org/10.3969/j.issn.1003-7985.2014.04.001.

[24] C.E. Perkins, E.M. Royer, Ad-hoc on-demand distance vector routing, in: The Workshop on Mobile Computing Systems & Applications, 2002, pp. 94–95.
[25] M. Al-Rabayah, R. Malaney, A new scalable hybrid routing protocol for vanets, IEEE Trans. Veh. Technol. 61 (6) (2012) 2625–2635, http://dx.doi.org/10.1109/TVT.2012.2198837.
[26] M. Slavik, I. Mahgoub, Spatial distribution and channel quality adaptive protocol for multihop wireless broadcast routing in vanet, IEEE Trans. Mob. Comput. 12 (4) (2013) 722–734, http://dx.doi.org/10.1109/TMC.2012.42.
[27] M.D. Felice, L. Bedogni, L. Bononi, Group communication on highways: An evaluation study of geocast protocols and applications, Ad Hoc Netw. 11 (3) (2013) 818–832, http://dx.doi.org/10.1016/j.adhoc.2012.09.011.
[28] C. Quadros, A. Santos, M. Gerla, E. Cerqueira, Qoe-driven dissemination of real-time videos over vehicular networks, Comput. Commun. 91–92 (C) (2016) 133–147, http://dx.doi.org/10.1016/j.comcom.2016.07.008.
[29] F. Li, Y. Wang, Routing in vehicular ad hoc networks: A survey, Veh. Technol. Mag. IEEE 2 (2) (2007) 12–22, http://dx.doi.org/10.1109/MVT.2007.912927.
[30] C. Lochert, H. Hartenstein, J. Tian, H. Fussler, D. Hermann, M. Mauve, A routing strategy for vehicular ad hoc networks in city environments, in: Intelligent Vehicles Symposium, 2003 Proceedings, IEEE, 2003, pp. 156–161, http://dx.doi.org/10.1109/IVS.2003.1212901.
[31] B. Karp, H.T. Kung, Gpsr: greedy perimeter stateless routing for wireless networks, in: International Conference on Mobile Computing and NETWORKING, 2000, pp. 243–254.
[32] S.H. Cha, K.W. Lee, H.S. Cho, Grid-based predictive geographical routing for inter-vehicle communication in urban areas, Int. J. Distrib. Sens. Netw. 2012 (3) (2012) 155–172, http://dx.doi.org/10.1155/2012/819497.
[33] B.D. Greenshields, A study of traffic capacity, Proc.h.r.b (1935) 14, http://dx.doi.org/10.3390/s16070974.

Daxin Tian is an associate professor with the School of Transportation Science and Engineering, Beihang University, Beijing, China. His current research interests include mobile computing, intelligent transportation systems, vehicular ad hoc networks, and swarm intelligent.

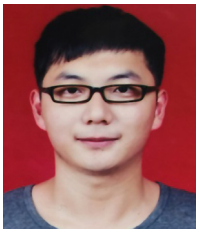

Chuang Zhang is currently working towards the master degree with the School of Transportation Science and Engineering, Beihang University, Beijing, China. His current research interests include multimedia communications and processing, and machine learning.

Xuting Duan is a lecturer with the School of Transportation Science and Engineering, Beihang University, Beijing, China. His current research interests include connected vehicles, vehicular ad hoc networks, and vehicular localization.

Yunpeng Wang is a professor with the School of Transportation Science and Engineering, Beihang University, Beijing, China. His current research interests include intelligent transportation systems, traffic safety, and vehicle infrastructure integration.

Jianshan Zhou is currently working towards the Ph.D. degree with the School of Transportation Science and Engineering, Beihang University, Beijing, China. His current research interests are focused on wireless communication, artificial intelligent system, and intelligent transportation systems.

Zhengguo Sheng is a lecturer with the Department of Engineering and Design, the University of Sussex, U.k. His current research interests include Cloud computing, Internet of things, Machine-to-Machine, Power line communications, Vehicle communications, Wireless sensor networks.